Hydrogen-Bonding and Polar Group Effects on Redox Potentials in Mo[HB(Me$_2$pz)$_3$](NO)(SR)$_2$[†,‡]

Jiong Huang,[§] Robert L. Ostrander,[∥] Arnold L. Rheingold,[∥] Yiuchong Leung,[§] and Marc Anton Walters*[,§]

Contribution from the Departments of Chemistry, New York University, New York, New York 10003, and University of Delaware, Newark, Delaware 19716

Received February 11, 1994[⊗]

Abstract: A series of Mo thiolate complexes with the formula Mo[HB(Me$_2$pz)$_3$](NO)(SR)$_2$, R = Et (**1**), Bu^n (**2**), $CH_2CONHCH_3$ (**3**), $CH_2CON(CH_3)_2$ (**4**), $C_2H_4CONHCH_3$ (**5**), and $C_2H_4CON(CH_3)_2$ (**6**), have been studied using the methods of cyclic voltammetry, IR and resonance Raman spectroscopy, and for **3** and **5**, X-ray crystallography. The polar groups of the thiolate ligands exert an influence on the redox potentials reflected in the $E_{1/2}$ series for the Mo^{2+}/Mo^{3+} redox couple recorded in CH_3CN: **2**, –0.960; **1**, –0.940; **5**, –0.820; **6**, –0.750; **4**, –0.740; **3**, –0.643 V (relative to SCE). The corresponding frequencies for the ν(NO) band increase in the same order: **2**, 1658; **1**, 1661; **5**, 1663; **6**, 1664; **4**, 1669; **3**, 1671 cm^{-1}, showing a correlation between the redox potential and the nitrosyl frequency. Complex **3** belongs to space group $P\bar{1}$ with a = 10.564(4) Å, b = 12.160(5) Å, c = 12.478(6) Å, α = 110.27(3)°, β = 92.64(4)°, γ = 105.96(3)°, V = 1427.8(10) Å^3, and Z = 2. Complex **5** belongs to space group $P\bar{1}$ with a = 9.565(8) Å, b = 11.480(9) Å, c = 18.510(20) Å, α = 73.35(8)°, β = 77.38(8)°, γ = 88.17(7)°, v = 1899.2(31) Å^3, and Z = 2. Complex **3** exhibits a single *intraligand* N–H···S hydrogen bond in the solid state, with even more extensive N–H···S bonding evident in solution. By contrast **5** forms an *interligand* N–H···O hydrogen bond which precludes the formation of N–H···S hydrogen bonds. Within the series of thiolate complexes examined, simple charge–dipole interactions appear to induce redox potential shifts of several hundred millivolts. The largest shift is observed in **3**, which forms intraligand hydrogen bonds. These results underscore the likely importance of charge–dipole interactions involving ligated thiolate sulfur in iron–sulfur redox proteins. From this perspective, hydrogen bonding and its effects on redox potential should be viewed in terms of electrostatic influence exerted on the electronic structure of the redox center.

Introduction

The effect of hydrogen bonding on redox potentials in cysteine–metal electron-transfer proteins[1-6] and their transition metal model compounds[7-16] has been the subject of extensive discussion over the course of nearly two decades. Model compounds have been synthesized incorporating simple thiolates or polypeptide ligands where, for example, cys-*x*-*y*-cys serves to mimic the geometry of the rubredoxin active site.[8-10] Results from studies using dicysteinate polypeptide ligands suggest that *intraligand* N–H···S hydrogen bonds are responsible for the relatively positive redox potentials of the model complexes. Until recently, there were no accurate measurements of N–H···S hydrogen-bonding distances and spatial orientations in transition metal model complexes. Such data have now been presented in the form of X-ray crystallographic results from our laboratory[17-20] and that of Nakamura and co-workers.[13,14] To date, published X-ray crystallographic data on N–H···S hydrogen-bonding complexes have been available only for phenylthiolate complexes. However, in redox protein model compounds, conjugation between sulfur and the phenyl ring is undesirable because it allows a π orbital conjugation and therefore inductive effects between the hydrogen bond donor and acceptor.[21]

This report details work on a new set of alkanethiolate complexes, Mo[HB(Me$_2$pz)$_3$](NO)(SR)$_2$ (pz = pyrazole), that are particularly well suited for the study of N–H···S hydrogen bonding and its effects on redox potential (tris(3,5-dimethylpyrazolyl)hydroborate = HB(Me$_2$pz)$_3$). A variety of thiolate ligands $[SR]^-$ are included in this study: R = (i) Et, ethanethiolate; (ii) Bu^n, *n*-butanethiolate; (iii) $CH_2CONHCH_3$, *N*-methylmercaptoacetamide; (iv) $CH_2CON(CH_3)_2$, *N,N*-dimethylmercaptoacetamide; (v) $C_2H_4CONHCH_3$, *N*-methylmercaptopropionamide;

† Bis(thiolato)(nitrosyl)[tris(3,5-dimethylpyrazolyl)borato]molybdenum.

‡ This work was presented in preliminary form at the Sixth International Conference on Bioinorganic Chemistry, August 22–27, 1993, San Diego, CA.

§ New York University.

∥ University of Delaware.

⊗ Abstract published in *Advance ACS Abstracts*. June 15, 1994.

(1) Adman, E. *Biochim. Biophys. Acta* **1979**, *549*, 107–144.
(2) Backes, G.; Mino, Y.; Loehr, T. M.; Meyer, T. E.; Cusanovich, M. A.; Sweeney, W. V.; Adman, E. T.; Sanders-Loehr, J. *J. Am. Chem. Soc.* **1991**, *113*, 2055–2064.
(3) Adman, E.; Watenpaugh, K. D.; Jensen, L. H. *Proc. Natl. Acad. Sci. U.S.A.* **1975**, *72*, 4854–4858.
(4) Watenpaugh, K. D.; Sieker, L. C.; Jensen, L. H. *J. Mol. Biol.* **1979**, *131*, 509–522.
(5) Adman, E. T.; Sieker, L. C.; Jensen, L. H. *J. Mol. Biol.* **1991**, *217*, 337–352.
(6) LeGall, J. *J. Mol. Biol.* **1987**, *197*, 525–541.
(7) Maskiewicz, R.; Bruice, T. *J. Chem. Soc., Chem. Commun.* **1978**, 703–704.
(8) Ueyama, N.; Nakata, M.; Fuji, M.-A.; Terakawa, T.; Nakamura, A. *Inorg. Chem.* **1985**, *24*, 2190–2196.
(9) Nakata, M.; Ueyama, N.; Fuji, M.-A.; Nakamura, A.; Wada, K.; Matsubara, H. *Biochim. Biophys. Acta* **1984**, *788*, 306–312.
(10) Nakamura, A.; Ueyama, N. In *Metal Clusters in Proteins*; Que, L., Ed.; ACS Symposium Series 372; American Chemical Society: Washington, DC, 1988: pp 293–301.
(11) Krüger, H.-J.; Peng, G.; Holm, R. H. *Inorg. Chem.* **1991**, *30*, 734–742.
(12) Hill, C. L.; Renaud, J.; Holm, R. H.; Mortenson, L. E. *J. Am. Chem. Soc.* **1977**, *99*, 2549–2557.
(13) Ueyama, N.; Okamura, T.-A.; Nakamura, A. *J. Am. Chem. Soc.* **1992**, *114*, 8129–8137.
(14) Nakamura, A.; Ueyama, N.: Okamura, T.-A.; Takamizawa, S. *J. Inorg. Biochem.* **1993**, *51*, 30.
(15) Huang, J.; Walters, M. A. *J. Inorg. Biochem.* **1993**, *51*, 24.
(16) DePamphilis, B. V.; Averill, B. A.; Herskovitz, T.; Que, L., Jr.; Holm, R. H. *J. Am. Chem. Soc.* **1974**, *96*, 4159–4167.
(17) Walters, M. A.; Dewan, J. C.; Min, C.; Pinto, S. *Inorg. Chem.* **1991**, *30*, 2656–2662.
(18) Chung, W. P.; Dewan, J. C.; Walters, M. A. *J. Am. Chem. Soc.* **1991**, *113*, 525–530.
(19) Chung, W. P.; Dewan, J. C.; Walters, M. A. *Inorg. Chem.* **1991**, *30*, 4280–4282.
(20) Walters, M. A.; Chung, W.; Huang, J. *J. Inorg. Biochem.* **1991**, *43*, 263.
(21) Reynolds, W. F. In *Progress in Physical Organic Chemistry*; Taft, R. W., Ed.; Wiley: New York, 1983; Vol 14, pp 165–203.

0002-7863/94/1516-6769$04.50/0

and (vi) $C_2H_4CON(CH_3)_2$, *N,N*-dimethylmercaptopropionamide. For one member of this series we observe amide thiolate N–H···S hydrogen bonding in both the solid and solution states. More importantly, relative to alkylthiolate complexes, significant positive shifts occur in the redox potentials of all the amide thiolate complexes. These results are likely to be of importance in the development of a quantitative model of the effect on redox potential of ligand hydrogen bonds and polar groups in proximity to redox centers in metalloproteins.

Experimental Section

All reactions, unless otherwise specified, were carried out in dry, oxygen-free solvents under nitrogen.

In column chromatography, silica gel G, 10–40 μm (EM Laboratories Inc.) was used with 10% THF in CH_2Cl_2 as the eluant.

Syntheses of Ligands and Complexes. Potassium hydrotris(3,5-dimethylpyrazole)borate, $K[BH(Me_2pz)_3]$, was synthesized by published methods.[22] The complex $Mo[BH(Me_2pz)_3](NO)I_2$ was synthesized by the method of McCleverty and co-workers.[23]

$Mo[BH(Me_2pz)_3](NO)(SC_2H_5)_2$ (1). NaSEt (0.192 g, 2.34 mmol) and $Mo[BH(Me_2pz)_3](NO)I_2$ (0.75 g, 0.98 mmol) were combined in THF (50 mL) and refluxed for 30 h. The solution was then filtered and the solvent evaporated to dryness. The solid thus obtained was dissolved in 50 mL of heptane. This solution was filtered and concentrated under vacuum to near saturation and maintained at –35 °C to give microcrystals (yield: 64%). NMR (ppm) ($CDCl_3$): 5.88 and 5.66 (pz, 4-H), 4.10 (SCH_2), 2.67, 2.47, 2.41, 2.31 (pz, CH_3), 1.32 (CH_3). UV–vis ($CHCl_3$): 356, 468 nm. Anal. Calcd for $C_{19}H_{32}BMoN_7OS_2{\cdot}0.2C_7H_{16}$: C, 43.33; H, 6.27; N, 17.34. Found: C, 43.33; H, 6.36; N, 17.55.

$Mo[BH(Me_2pz)_3](NO)(SBu^n)_2$ (2).[24] $Mo[BH(Me_2pz)_3](NO)I_2$ (0.75 g, 0.98 mmol) was dissolved with ^nBuSH (0.50 mL) in 50 mL of heptane and refluxed for 40 h. The solution was filtered, concentrated to about 10 mL, and maintained at –35 °C, to give black crystals of the monosubstitution product $Mo[BH(Me_2pz)_3](NO)I(SBu^n)$ (yield: 73%).

$Mo[BH(Me_2pz)_3](NO)I(SBu^n)$ (0.42 g, 0.66 mmol), $Ag(CH_3CO_2)$ (0.13 g), and $HSBu^n$ (0.30 mL) were added to heptane (50 mL) and again refluxed for 40 h. The solution was filtered, concentrated under vacuum, and chilled to –35 °C, yielding dark red microcrystals of $Mo[BH(Me_2pz)_3](NO)(SBu^n)_2$ (yield: 78%).

***N*-Methylmercaptoacetamide.** Ethyl 2-mercaptoacetate (10.0 g, 83.2 mmol) and methylamine (20.1 mL, 40% aqueous solution, 250 mmol) were combined and stirred overnight. The excess reagent was removed by distillation under reduced pressure on a hot water bath, leaving the product as a clear colorless liquid (yield: 97%). NMR(ppm) (DMSO-d_6): 7.91 (NH), 3.03 ($N(CH_3)$), 2.55 (SCH_2). IR(cm^{-1}) (thin film): 2553.1 ν(SH), 1653.1 ν(CO).

***N,N*-Dimethylmercaptoacetamide.** Thiolacetic acid (1.5 mL, 20.7 mmol) was combined with KOH (1.16 g, 20.7 mmol) in 15 mL of EtOH, and the mixture was added to 2-chloro-*N,N*-dimethylacetamide (2.01 g, 16.5 mmol) and refluxed for 3 h. The solution was filtered, followed by extraction using $CHCl_3$ (100 mL) and H_2O (30 mL). The $CHCl_3$ layer was dried over $CaSO_4$ and filtered, and the solvent was evaporated to give the thiol ester as a yellow liquid (yield: 94.8%). NMR(ppm) (DMSO-d_6): 3.84 (CH_2), 3.20, 2.82 ($N(CH_3)$), 2.38 ($COCH_3$). IR (cm^{-1}) (thin film): 1693.7 and 1651.6 ν(CO) for MeCOS and $CON(CH_3)_2$. The thiol ester, in 20 mL of MeOH, was combined with KOH (1.76 g, 31.4 mmol) in 30 mL of MeOH and refluxed for 4 h. The pH of the solution was adjusted to 2.0 using HCl, followed by filtration and solvent evaporation under vacuum. The next extraction step was carried out in the air using 50 mL of $CHCl_3$ and 40 mL of H_2O. The $CHCl_3$ layer was dried over $CaSO_4$ and filtered, and the solvent was removed on a Rotovap (yield: 54.2%). NMR(ppm) (DMSO-d_6): 3.41 (CH_2), 3.02, 2.85 ($N(CH_3)_2$), and 2.78 (SH). IR(cm^{-1}) (thin film): 2537.5 ν(SH); 1644.5 ν(CO).

In an alternative synthetic approach, dimethylamine was dissolved in MeOH and refluxed with ethyl-2-mercaptoacetate for 1 day. The solvent and excess dimethylamine were removed by evaporation under vacuum to yield the pure product *N,N*-dimethylmercaptoacetamide.

***N*-Methylmercaptopropionamide.**[25] Ethyl 3-mercaptopropionate (10.0 g, 74.0 mmol) was added to a flask containing methylamine (20 mL, 40% aqueous solution, 224 mmol) and stirred overnight. The solvent was removed by distillation under reduced pressure. The product was obtained as a clear liquid, which crystallized at room temperature (mp 35 °C) (yield: 98.8%). NMR(ppm) (DMSO-d_6): 7.85 (NH), 2.61 (SCH_2), 2.54 ($N(CH_3)$), 2.33 (CH_2CO). IR(cm^{-1}) (thin film): 2552.3 ν(SH); 1649.2 ν(CO).

***N,N*-Dimethylmercaptopropionamide.** Ethyl 3-mercaptopropionate (10.0 g, 74.0 mmol) and liquid $NH(CH_3)_2$ (40 mL) were combined in methanol (60 mL). The solution was refluxed for 4 days with the addition of $NH(CH_3)_2$ to maintain the solution volume followed by solvent evaporation under vacuum leaving a colorless liquid (yield: 84%). NMR-(ppm) ($CDCl_3$): 3.01 and 2.95 ($N(CH_3)_2$), 2.80 (CH_2CO) and 2.64 (SCH_2), 2.30 (SH). IR(cm^{-1}) (thin film): 2544.5, ν(SH); 1644.5, ν(CO).

$Mo[BH(Me_2pz)_3](NO)(SCH_2CONHCH_3)_2$ (3). *N*-methylmercaptoacetamide (1.25 g, 11.9 mmol) and sodium (0.274 g, 11.9 mmol) were combined in methanol (30 mL) to form $NaSCH_2CONHCH_3$. The solvent was removed under vacuum. The product was stirred with THF overnight to extract excess alcohol. The THF was then decanted and the remaining solid dried under vacuum leaving a white powder (yield: 1.20 g, 79.4%). NMR(ppm) (DMSO-d_6): 8.64(NH), 2.84 (SCH_2), 2.51 ($N(CH_3)$). $NaSCH_2CONHCH_3$ (0.75 g, 5.91 mmol) and $Mo[BH(Me_2pz)_3](NO)I_2$ (1.5 g, 1.95 mmol) were added to THF (100 mL), and the solution was refluxed for 2 days. The solvent was removed under vacuum on a hot water bath followed by redissolution in CH_2Cl_2 (60 mL) and filtration to remove NaI. Concentration to 10 mL under vacuum and addition of hexane (60 mL) induced crystallization after 2 days at –10 °C to give dark red microcrystals (yield: 83%). Crystals suitable for single-crystal X-ray diffraction were grown by the slow diffusion of hexane into the CH_2Cl_2 solution. NMR(ppm) ($CDCl_3$): 6.23 (NH), 6.01 and 5.78 (pz, 4-H), 4.51 (SCH_2), 2.60 and 2.63 ($N(CH_3)$), 2.55, 2.49, 2.37, and 2.33 (pz, CH_3). UV–vis ($CHCl_3$): 374, 464 nm. Anal. Calcd for $C_{21}H_{34}BMoN_9O_3S_2{\cdot}0.3CH_2Cl_2$: C, 38.93; H, 5.30; N, 19.19. Found: C, 38.69; H, 4.89; N, 19.63.

$Mo[BH(Me_2pz)_3](NO)[SCH_2CON(CH_3)_2]_2$ (4). *N,N*-Dimethylmercaptoacetamide was converted to its sodium salt as above (yield: 59.1%). NMR(ppm) (DMSO-d_6): 3.15 (CH_2), 2.70 and 2.80 ($N(CH_3)_2$). $NaSCH_2CON(CH_3)_2$ (0.310 g, 2.20 mmol) and $Mo[BH(Me_2pz)_3](NO)I_2$ (0.501 g, 0.650 mmol) were combined in THF (50 mL) and refluxed for 2 days. The solvent was evaporated under vacuum, and the product was redissolved in $CHCl_3$ (40 mL) followed by filtration. The solvent was removed under vacuum, leaving the product as a dark brown powder. Purification was carried out by column chromatography with collection of the main fraction on the basis of UV–vis features followed by solvent evaporation. The residue was recrystallized from CH_2Cl_2/hexane, affording dark green crystals (yield: 32.7%). NMR(ppm) ($CDCl_3$): 6.00 and 5.78 (pz, 4-H), 4.80 (SCH_2), 3.04, 2.93 ($N(CH_3)_2$), 2.34, 2.45, 2.48, 2.64 (pz, CH_3). UV–vis ($CHCl_3$): 352, 468 nm. Anal. Calcd for $C_{23}H_{38}BMoN_9O_3S_2{\cdot}0.3CH_2Cl_2$: C, 40.24; H, 5.55; N, 18.13. Found: C, 40.07; H, 5.89; N, 18.74.

$Mo[BH(Me_2pz)_3](NO)(SC_2H_4CONHCH_3)_2$ (5). The sodium salt of *N*-methylmercaptopropionamide was generated in methanol. The resulting white solid, $NaSC_2H_4CONHCH_3$, was washed with THF and vacuum-dried (yield: 84%). NMR(ppm) (DMSO-d_6): 10.21 (NH), 2.55 (NCH_3), 2.45 (CH_2), 2.13 (SCH_2). $NaSC_2H_4CONHCH_3$ (0.525 g, 3.73 mmol) and $Mo[BH(Me_2pz)_3](NO)I_2$ (1.01 g, 1.31 mmol) were combined in THF (50 mL) and refluxed for 2 days. The solution was then filtered and the solvent removed under vacuum on a hot water bath. Recrystallization from acetonitrile/pentane gave brown crystals (yield: 63.7%). Crystals suitable for single-crystal X-ray diffraction were grown from dichloromethane/hexane by slow evaporation of solvent. NMR(ppm) ($CDCl_3$): 6.25 (NH), 5.98 and 5.74 (pz, 4-H), 4.5 and 4.25 (SCH_2), 2.78 and 2.76 ($N(CH_3)$), 2.63 and 2.61 (CH_2), 2.60, 2.48, 2.39, 2.32 (pz, CH_3). UV–vis ($CHCl_3$): 360, 468 nm. Anal. Calcd for $C_{23}H_{38}BMoN_9O_3S_2{\cdot}1.25CH_2Cl_2$: C, 38.02; H, 5.32; N, 16.47. Found: C, 38.17; H, 4.70; N, 15.93.

$Mo[BH(Me_2pz)_3](NO)[SC_2H_4CON(CH_3)_2]_2$ (6). Sodium *N,N*-dimethylmercaptopropionamide was prepared as above with a yield of 58%. $NaSC_2H_4CON(CH_3)_2$ (0.33 g, 2.13 mmol) and $Mo[BH(Me_2pz)_3](NO)I_2$ (0.62 g, 0.818 mmol) were combined in 50 mL of THF and refluxed for 2 days. The solvent was evaporated under vacuum, and the product was redissolved in $CHCl_3$ (40 mL). The solution was filtered and the solvent removed under vacuum. The product was purified by column

(22) Trofimenko, S. *J. Am. Chem. Soc.* **1967**, *89*, 6288–6294.
(23) Reynolds, S. J.; Smith, C. F.; Jones, C. J.; McCleverty, J. A. *Inorg. Syn.* **1983**, *23*, 4–9.
(24) McCleverty, J. A.; Drane, A. S.; Bailey, N. A.; Smith, J. M. A. *J. Chem. Soc., Dalton Trans.* **1983**, 91–96.
(25) Houghten, R.; Li, C. H. *Anal. Biochem.* **1979**, *98*, 36–46.

Table 1. Crystal Data for Mo[BH(Me$_2$pz)$_3$](NO)(SCH$_2$CONHCH$_3$)$_2$ (3) and Mo[BH(Me$_2$pz)$_3$](NO)(SC$_2$H$_4$CONHCH$_3$)$_2$·1.36CH$_2$Cl$_2$ (5)

	(a) Crystal Parameters	
formula	$C_{21}H_{34}BMoN_9O_3S_2$ (3)	$C_{23}H_{38}BMoN_9O_3S_2$·1.36CH_2Cl_2 (5)
formula weight	631.4	774.9[a]
cryst system	triclinic	triclinic
space group	$P\bar{1}$	$P\bar{1}$
a, Å	10.564(4)	9.565(8)
b, Å	12.160(5)	11.480(9)
c, Å	12.478(6)	18.510(20)
α, deg	110.27(3)	73.35(8)
β, deg	92.64(4)	77.38(8)
γ, deg	105.96(3)	88.17(7)
V, Å^3	1427.8(10)	1899.2(31)
Z	2	2
D(calc), g cm^{-3}	1.469	1.355[a]
μ(Mo Kα), mm^{-1}	0.645	0.684[a]
temp, K	298	235
cryst size, mm	0.25 × 0.32 × 0.62	0.30 × 0.42 × 0.46
cryst color	deep red	deep red
	(b) Data Collection	
diffractometer	Siemens P4	
monochromator	oriented graphite	
radiation	Mo Kα	
wavelength, Å	0.71073	
2θ limits, deg	$4 < 2\theta < 52$	$4 < 2\theta < 45$
decay	~1%	~1%
no. of rflns collcd	5603	7114
no. of independt rflns, $F_o \geq 5\sigma(F_o)$	4508	5242
	(c) Refinement	
$R(F)$, %[b]	4.10	8.04
$R_w(F)$, %[c]	5.84	10.18
GOF	1.34	1.89
$\Delta(\rho)$, e Å^{-3}	+0.47, −0.53	+1.91, −1.68
N_o/N_v	13.5	12.8

[a] Values of the formula weight, calculated density, and linear absorption of **5** reflect the fractional occupation factor of the solvent molecules. [b] $R = \sum(|F_o| - |F_c|)/\sum|F_o|$. [c] $Rw = \{\sum w(|F_o| - |F_c|)^2/\sum w|F_o|^2\}^{1/2}$; $w^{-1} = \sigma^2F_o + gF_o^2$.

Table 2. Selected Bond Distances and Angles for Mo[BH(BH(Me$_2$pz)$_3$](NO)(SCH$_2$CONHCH$_3$)$_2$ (3)

	Bond Distances (Å)		
Mo–S(1)	2.347(2)	Mo–N(7)	1.762(3)
Mo–S(2)	2.348(2)	S(1)–C(16)	1.834(4)
Mo–N(1)	2.222(4)	S(2)–C(19)	1.813(4)
Mo–N(3)	2.219(4)	N(7)–O(1)	1.204(5)
Mo–N(5)	2.241(3)	N(9)···S(2)	2.971(4)
	Bond Angles (deg)		
S(1)–Mo–S(2)	102.8(1)	N(1)–Mo–N(3)	76.6(2)
S(1)–Mo–N(1)	164.9(1)	N(1)–Mo–N(5)	86.3(1)
S(1)–Mo–N(3)	90.1(1)	N(1)–Mo–N(7)	96.4(2)
S(1)–Mo–N(5)	85.5(1)	N(3)–Mo–N(5)	85.4(1)
S(1)–Mo–N(7)	92.7(1)	N(3)–Mo–N(7)	98.4(2)
S(2)–Mo–N(1)	88.6(1)	N(5)–Mo–N(7)	175.8(2)
S(2)–Mo–N(3)	161.4(1)	Mo–S(1)–C(16)	111.2(2)
S(2)–Mo–N(5)	82.4(1)	Mo–S(2)–C(19)	113.1(2)
S(2)–Mo–N(7)	94.4(1)	Mo–N(7)–O(1)	176.9(4)

Table 3. Selected Bond Distances and Angles for Mo[BH(Me$_2$pz)$_3$](NO)(SC$_2$H$_4$CONHCH$_3$)$_2$·1.36CH$_2$Cl$_2$ (5)

	Bond Distances (Å)		
Mo–S(1)	2.337(2)	Mo–N(9)	1.791(6)
Mo–S(2)	2.345(2)	S(1)–C(16)	1.824(10)
Mo–N(1)	2.210(6)	S(2)–C(20)	1.814(9)
Mo–N(3)	2.222(5)	N(9)–O(3)	1.157(8)
Mo–N(5)	2.256(6)	N(7)···O(2)	2.824(8)
	Bond Angles (deg)		
S(1)–Mo–S(2)	104.3(1)	N(1)–Mo–N(3)	76.3(2)
S(1)–Mo–N(1)	162.7(2)	N(1)–Mo–N(5)	85.9(2)
S(1)–Mo–N(3)	88.8(2)	N(1)–Mo–N(9)	96.5(2)
S(1)–Mo–N(5)	84.2(2)	N(3)–Mo–N(5)	85.7(2)
S(1)–Mo–N(9)	93.8(2)	N(3)–Mo–N(9)	96.1(2)
S(2)–Mo–N(1)	88.9(1)	N(5)–Mo–N(9)	177.3(2)
S(2)–Mo–N(3)	163.3(2)	Mo–S(1)–C(16)	111.5(3)
S(2)–Mo–N(5)	85.5(1)	Mo–S(2)–C(20)	110.7(2)
S(2)–Mo–N(9)	93.3(2)	Mo–N(9)–O(3)	177.6(6)

chromatography and the desired fraction collected on the basis of its UV–vis spectrum. UV–vis ($CHCl_3$): 358, 468 nm. The solvent was evaporated leaving a dark green powder, which was washed with hexane, dried under vacuum, and recrystallized from dichloromethane/hexane by slow evaporation of solvent (yield: 19.5%). NMR(ppm) ($CDCl_3$): 6.00 and 5.75 (pz, 4-H), 4.27 (SCH_2), 3.02 and 2.95 ($N(CH_3)_2$), 2.62 and 2.35 (CH_2), 2.50, 2.48, 2.32, 2.30 (pz, CH_3). Anal. Calcd for $C_{25}H_{42}BMoN_9O_3S_2$·0.2CH_2Cl_2·0.2C_6H_{14}: C, 43.93; H, 6.31; N, 17.47. Found: C, 44.06; H, 6.39; N, 17.40.

Proton NMR data were collected by using Varian Gemini-200 and General Electric QE-300 spectrometers.

IR data were collected at 4-cm^{-1} resolution in a 5 mm path length cell on a Nicolet 5DXB spectrometer. All samples were prepared in CH_2Cl_2, $CHCl_3$, and/or $CDCl_3$. Variable temperature measurements were made by using a SPECAC variable temperature cell, P/N 21.500 equipped with CaF_2 windows, with a 5-mm path length.

Resonance Raman data were collected at room temperature with 10-cm^{-1} spectral slit width. Samples were prepared as saturated CH_2Cl_2 solutions. The experiment was carried out in the backscattering geometry in which sample solutions were spun in 8-in. ultrathin-walled NMR tubes (Wilmad).[26] A description of the experimental apparatus and data processing software has been previously provided.[17]

Electronic absorption data were obtained using a Hewlett-Packard 8452A diode array spectrometer controlled by a Zenith Data Systems ZDE-1217-AO computer.

Elemental analyses were performed by Galbraith Laboratories, Inc., Knoxville, TN.

Cyclic voltammetry was carried out with a Pine Instruments AFRDF4 potentiostat. The measurements were made in dry acetonitrile, methanol, and chloroform under N_2 in a Vacuum Atmospheres glovebox. Experimental details are given in Table 5.

X-Ray Structure Determinations. Crystallographic data for **3** and **5** are collected in Table 1, and selected bond lengths and angles are given in Tables 2 and 3. Preliminary photographic characterization showed that both crystals possessed $\bar{1}$ Laue symmetry. Although the shape of the crystal of **3** was not as uniform as that of **5**, azimuthal ψ scans showed angular intensity deviations of less than 10% and the linear absorption

(26) Walters, M. A. *Appl. Spectrosc.* **1983**, *37*, 299–300.

coefficients for both crystals were low; thus no absorption corrections were used for either crystal. Although far from ideal, the quality of the X-ray diffraction data set of **3**, with its relatively large *R* factor and estimated standard deviations, does provide important connectivity information. We, however, eschew quantitative spectroscopic predictions based on the solid-state data.

Both structures were solved by direct methods and completed by difference Fourier synthesis. All non-hydrogen atoms were refined with anisotropic thermal parameters. All hydrogen atoms were treated as idealized, updated isotropic contributions. Two dichloromethane solvent molecules were located in **5**, having refined partial occupation factors of 0.69 and 0.65, respectively. The Cl atoms of the solvent molecules in **5** form Cl···H interactions, which contribute to crystal packing forces. Computations were made with the *SHELXTL PLUS* (4.27) program library (G. Sheldrick, Siemens XRD, Madison, WI).

Results and Discussion

Syntheses. Several criteria led to the selection of the complexes reported here as models for N–H···S interactions in redox proteins. Of primary importance was the formation of N–H···S hydrogen bonds that could be observable both in the solid state by X-ray crystallography and in solution by spectroscopic methods. We expected that this aim could be best achieved in complexes designed to form intramolecular hydrogen bonds. Classical studies[27] have shown that intramolecular hydrogen bonds are favored in solvents of low polarity. Therefore, neutral compounds, soluble in liquids of low polarity, were expected to be most suitable. Finally, we wished to avoid complexes in which the functional groups of interest would be linked both through hydrogen bonding and π bond conjugation, as occurs when amino- or amidophenylthiolate ligands are employed.

Several years ago McCleverty and co-workers[24] reported on some redox active tris-pyrazolyl borate complexes, $Mo[BH(Me_2pz)_3]NO(SR)_2$, where R = ^{n}Bu, Ph. These complexes satisfied the requirements mentioned above, with regard to charge and solvent compatibility. Our adaptation of this system involved the substitution of ligands whose R groups contained terminal secondary and tertiary amides, which we hoped would interact with sulfur to provide a quantitative measure of the effect of amide–thiolate hydrogen bonding on the redox potentials of the complexes.

We employed the set of ligands (i) SEt, (ii) SBu^n, (iii) $SCH_2CONHCH_3$, (iv) $SCH_2CON(CH_3)_2$, (v) $SC_2H_4CONHCH_3$, and (vi) $SC_2H_4CON(CH_3)_2$.

McCleverty[24] reported that the formation of dithiolate complexes required two steps:

$$Mo[BH(Me_2pz)_3]I_2(NO) + RSH \rightarrow Mo[BH(Me_2pz)_3]I(NO)(SR) \quad (1)$$

$$Mo[BH(Me_2pz)_3]I(NO)(SR) + Ag(CH_3CO_2) + RSH \rightarrow Mo[BH(Me_2pz)_3](NO)(SR)_2 \quad (2)$$

We found that with the exception of the butanethiolate derivative, which was prepared by the published method,[24] the dithiolate complexes were easily obtained by refluxing the appropriate sodium thiolate salt, NaSR, with $Mo[BH(Me_2pz)_3](NO)(I)_2$ in THF.

A priori, we thought the ligands $SCH_2CONHCH_3$ and $SC_2H_4CONHCH_3$ would be likely to exhibit the desired *intraligand* hydrogen bonding within the Mo complex. In analogy with compounds that cyclize with the formation of a covalent bond,[28] we expected to acquire five- and six-membered rings through the formation of an intramolecular hydrogen bond.

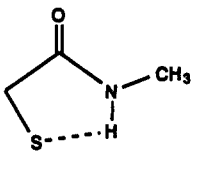

(iii)

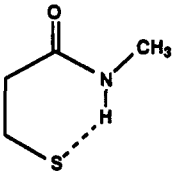

(v)

After this work was begun we came upon a series of infrared studies by Zuppiroli et al.[29–31] which showed that in CCl_4 the neutral compounds $HSCH_2CONHCH_3$ and $HSC_2H_4CONHCH_3$ adopted cyclized and extended structures, respectively.[29] In the solid state the neutral mercury complex $Hg(SR)_2$, in which $SR^- = [SCH_2CONHCH_3]^-$, has an *interligand* N–H···O hydrogen bond. This contrasts with the formation of an extended conformation stabilized by *intermolecular* N–H···O hydrogen bonds in the case where $SR^- = [SC_2H_4CONHCH_3]^-$.[30,31] With the thiolates $SCH_2CONHCH_3$ and $SC_2H_4CONHCH_3$ employed as ligands in $Mo[BH(Me_2pz)_3](NO)(SR)_2$ complexes we have observed a similar disparity between the mercaptoamide conformations (vide infra). Among the observed ligand geometries is one in **3** that involves an *intraligand* N–H···S hydrogen bond. Details of the solid-state conformations adopted by the ligands $SCH_2CONHCH_3$ and $SC_2H_4CONHCH_3$ in complexes **3** and **5**, respectively, are presented below.

Crystal Structures. The Mo–S bond lengths are 2.347(2) and 2.348(2) Å for **3** (Table 2) and 2.337(2) and 2.345(2) Å for **5** (Table 3). No average systematic bond length variation occurs as a function of N–H···S hydrogen bonding. Likewise, the average Mo–N_{pz} bond lengths are 2.228(4) for **3** and 2.229(6) Å for **5**. The distances between Mo and the coordinated nitrosyl N atom (Mo–NO) are 1.762(3) for **3** and 1.791(6) Å for **5**. Corresponding N–O bond lengths are 1.204(5) and 1.157(8) Å for complexes **3** and **5**, respectively.

It has been shown that torsional angle data can provide insight into the nature of the ligand–metal bonding in metal complexes. The results of an earlier study on a benzenethiolate complex can be applied to the interpretation of structural data of **3** and **5**. The complex $Mo[BH(Me_2pz)_3]NO(SPh)_2$[24] was crystallographically characterized by Roberts and Enemark.[32] The Mo–S bond lengths were found to be 2.3452(2) and 2.3702(9) Å, slightly longer on average than those of **3** and **5**. The benzenethiolate complex exhibited ON–Mo–S–C torsion angles of –16 and 168°. The close proximity of these angles to 0 and ±180° is indicative of good d–p orbital overlap, as would be expected in a $\{MoNO\}^4$ group whose d_{xz} and d_{yx} orbitals are filled.[32,33] (The $\{MoNO\}^4$ notation refers to the number of Mo d orbital and NO π^* orbital electrons in complex. This number describes the electron occupancy of the molecular orbitals and therefore allows a prediction of the geometries of ligand binding. The nomenclature and usage is discussed in the following: Hoffman, R.; Chen, M. M.-L.; Thorn, D. L. *Inorg. Chem.* **1977**, *16*, 503–511.) The torsion angle pairs for the complexes reported in our work are respectively 9.0(2)° (N(7)–Mo–S(1)–C(16)) and –6.2(2)° (N(7)–Mo–S(2)–C(19)) for **3** and 8.0(2)° (N(9)–Mo–S(1)–C(16)) and –13.1(1)° (N(9)–Mo–S(2)–C(20)) for **5**. These values are consistent with good d–p orbital overlap.

(27) Vinogradov, S. N.; Linnell, R. H. *Hydrogen Bonding*; Van Nostrand: New York, 1971; pp 11–15, 114–119.
(28) Carey, F. A.; Sundberg, R. *J. Advanced Organic Chemistry*; Plenum: New York, 1990; Part A, pp 163–167.
(29) Zuppiroli, G.; Perchard, C.; Baron, M. H.; de Loze, C. *J. Mol. Struct.* **1980**, *69*, 1–16.
(30) Perchard, C.; Zuppiroli, G.; Gouzerh, P.; Jeannin, Y.; Robert, F. *J. Mol. Struct.* **1981**, *72*, 119–129.
(31) Zuppiroli, G.; Perchard, C.; Baron, M. H.; de Loze, C. *J. Mol. Struct.* **1981**, *72*, 131–141.
(32) Roberts, S. A.; Enemark, J. H. *Acta Crystallogr.* **1989**, *C45*, 1292–1294.
(33) Ashby, M. T.; Enemark, J. H. *J. Am. Chem. Soc.* **1986**, *108*, 730–733.

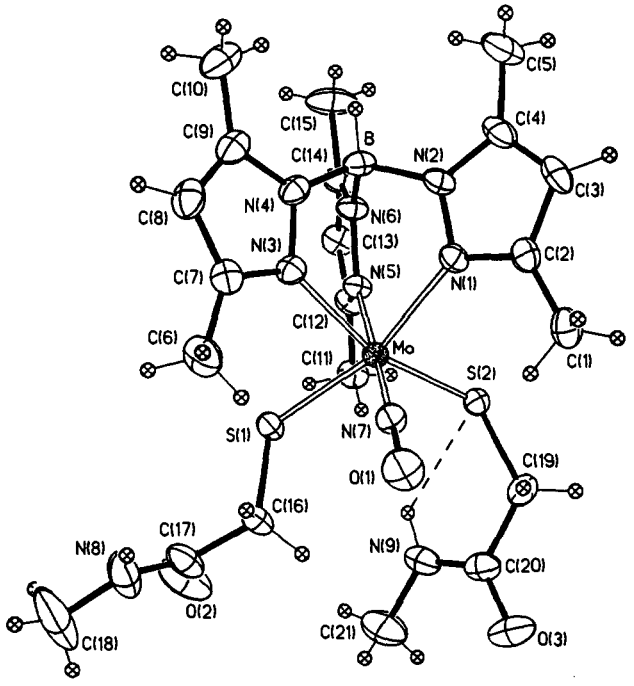

Figure 1. Molecular structure of $Mo[BH(Me_2pz)_3](NO)(SCH_2CONHCH_3)_2$, **3**, drawn with 35% ellipsoids.

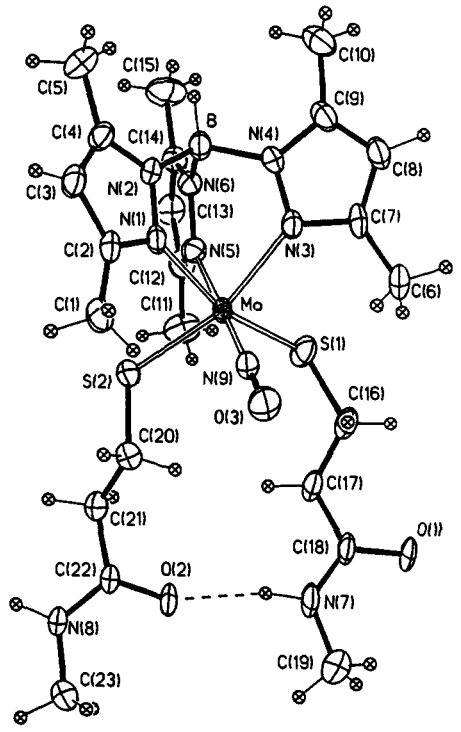

Figure 2. Molecular structure of $Mo[BH(Me_2pz)_3](NO)(SC_2H_4CONHCH_3)_2 \cdot 1.36CH_2Cl_2$, **5**, drawn with 35% ellipsoids.

Complex **3** exhibits a single N(9)–H···S(2) hydrogen bond with an N···S distance of 2.971(4) Å, which is unusually short,[34] but is consistent with the fact that the H-bond is bent.[35] The hydrogen bond results from ligand cyclization to form a five-membered ring in which the terminal amide group of the ligand is directly adjacent to the coordinated sulfur (Figure 1). The second thiolate ligand forms an *intermolecular* hydrogen bond, N(8)–H···O(3)*, with a neighboring ligand. In solution it is likely that the N–H···O linkage is disrupted, thus allowing a second *intraligand* hydrogen bond, N(8)–H···S(1), to form. Support for this interpretation is provided by infrared data discussed below. In complex **5** a single N(7)–H···O(2) *interligand* hydrogen bond is observed, with an N···O bond length of 2.824(8) Å. Its occurrence precludes the formation of *intraligand* N–H···S hydrogen bonds. (Figure 2) In the crystal the second carbonyl oxygen, O(1), is linked via an intermolecular hydrogen bond to N(8)* of an adjacent molecule. As in the case of complex **3**, the *intermolecular* linkage is probably disrupted in solution.

Vibrational Spectroscopy. We have determined the nature and extent of N–H hydrogen bonding in $CDCl_3$ solution from IR data.[27] For complexes **3** and **5** two ν(N–H) amide stretching bands are observed, corresponding to hydrogen-bonded (N–H_{bonded}) and non-hydrogen-bonded (N–H_{free}) N–H groups. The respective bands appear at 3401 and 3457 cm^{-1} for **3** and 3350 and 3463 cm^{-1} for **5** (Figure 3). The extent of hydrogen bonding is determined from the intensities of the ν(N–H_{free}) peaks of **3** and **5**, relative to those of *N*-methylmercaptopropionamide (2.2 mM) in $CDCl_3$, in which hydrogen bonding is absent. On this basis we have determined that the N–H···S or N–H···O hydrogen bonds of complexes **3** and **5** are dissociated to the extent of 6 and 53%, respectively.

In a hydrogen-bonded amide, the decrease in frequency of ν(N–H) relative to that of the unassociated form is expected to reflect the strength of the hydrogen bond.[36] We believe therefore that complexes **3** and **5** sustain their respective N–H···S and

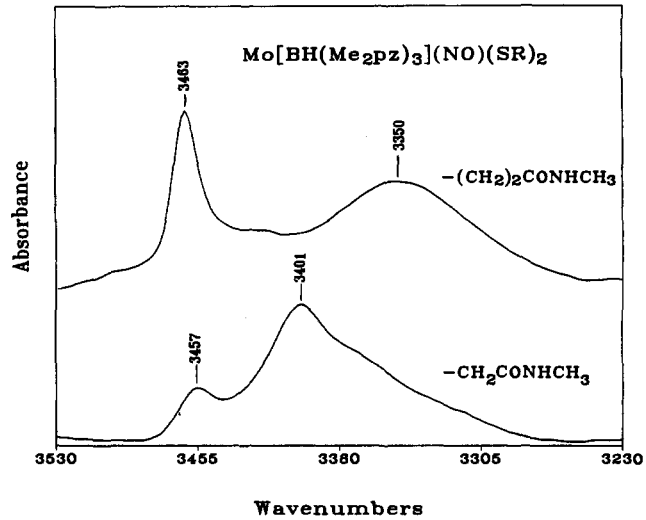

Figure 3. Infrared spectra showing the ν(N–H) bands for $Mo[BH(Me_2pz)_3](NO)(SC_2H_4CONHCH_3)_2$, **5** (top), and $Mo[BH(Me_2pz)_3](NO)(SCH_2CONHCH_3)_2$, **3** (bottom). Sample solutions were 2.0 mM in $CDCl_3$, 5-mm path length. Data were collected in 600 scans at 4-cm^{-1} resolution.

N–H···O hydrogen bonds in $CDCl_3$ solution. The N–H···O hydrogen bond is the stronger of the two[37,38] and therefore accounts for the ν(N–H) of **5** being 51 cm^{-1} lower than that found for complex **3**. On the basis of IR data, there is no evidence of N–H···S hydrogen bond formation in **5** in solution.

The hydrogen bond enthalpy for the neutral ligand $HSCH_2CONHCH_3$ was determined, using variable temperature IR data, to be –0.61 kcal/mol. As mentioned above, five-membered-ring formation is the only geometry that permits the formation of an internal hydrogen bond. No N–H···S hydrogen bonding was observed for the neutral ligand $HSC_2H_4CONHCH_3$, consistent with the studies of Zuppiroli et al.[29]

(34) Hamilton, W. C.; Ibers, J. A. *Hydrogen Bonding in Solids*; Benjamin: New York, 1968; Chapter 5.

(35) Huang, J.; Walters, M. A. Unpublished results. The N···S distances observed in tetrakis(*ortho*-aminobenzenethiolate) Co(II) and Fe(II) complexes are similar, ~3.0 Å, and belong to bent N–H···S hydrogen bonds.

(36) Fillaux, F.; de Lozé, C. *J. Chim. Phys. Physicochim. Biol.* **1972**, *69*, 36–44.

(37) Mino, Y.; Loehr, T. M.; Wada, K.; Matsubara, H.; Sanders-Loehr, J. *Biochemistry* **1987**, *26*, 8059–8065.

(38) Torchinsky, Yu. M. *Sulfur in Proteins*; Metzler, D., Trans. Ed.; Pergamon Press: New York, 1981; pp 8–10.

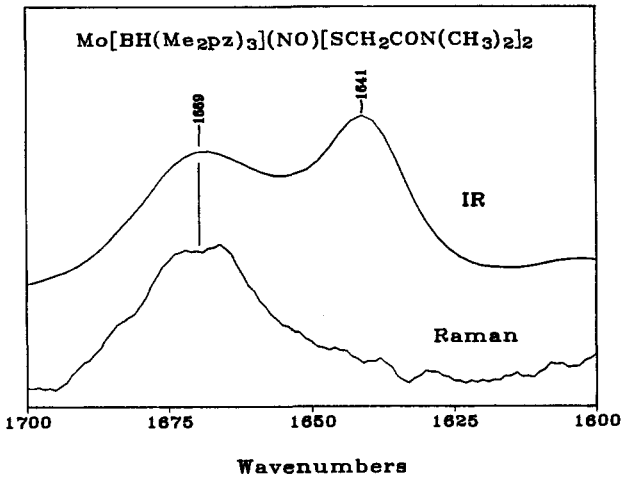

Figure 4. FTIR and Raman spectra of $Mo[BH(Me_2pz)_3](NO)[SCH_2CON(CH_3)_2]_2$, **4**, in CH_2Cl_2. Shown at the top is IR data: ν(NO) 1669 cm^{-1}, ν(CO) 1641 cm^{-1}. Conditions of data collection were as listed in Figure 3. Shown at the bottom is resonance Raman data: The ν(CO) peak is not observed. Raman data were collected using 4800-Å laser excitation at 100 mW, 10-cm^{-1} spectral slit width, 5 s/cm^{-1} stepping rate, and 180° backscattering geometry. Samples were contained in ultrathin NMR tubes and rotated in a gas turbine spinner during data acquisition.

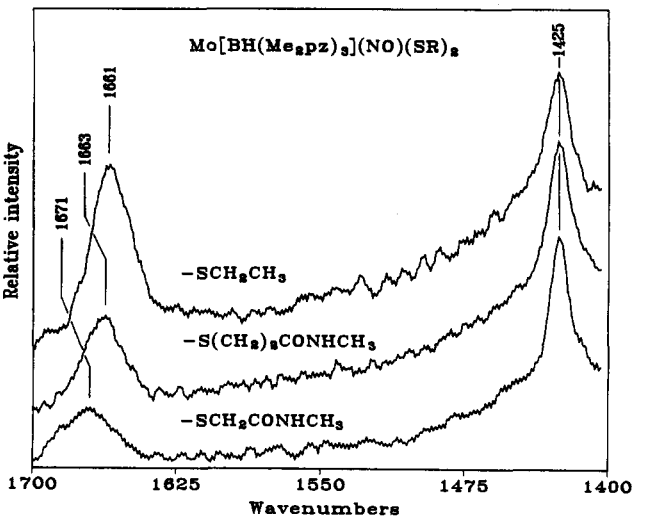

Figure 5. Raman spectra of $Mo[BH(Me_2pz)_3](NO)(SR)_2$ in CH_2Cl_2, where R = CH_2CH_3 (**1**), $C_2H_4CONHCH_3$ (**5**), and $CH_2CONHCH_3$ (**3**), respectively. Conditions for Raman data collection conditions are as listed in Figure 4.

In certain classes of complexes containing π-acid ligands it has been observed that redox potentials can be correlated with the vibrational frequencies of ν(CO) or ν(NO).[39] In the case of $Mo[HB(Me_2pz)_3](NO)(SR)_2$, the ν(NO) band has been shown[40] to respond to differences in the electron density of the metal coordination sphere. Higher frequencies are associated with more positive redox potentials, which would occur with a decrease in the electron density in the coordination sphere, through either an increased metal oxidation state or a decrease in the ligand field. McCleverty and co-workers proposed a linear relationship as expressed by the equation

$$\nu(NO) = \alpha E_{1/2} + N \qquad (3)$$

where N and α are constants.[40] They pointed out some limitations in the application of this equation to a mixed set of ligands because of the nonlinear behavior of thiolates relative to, for example, phenolates and halides. This nonlinear behavior was ascribed to $p\pi(S) \rightarrow d\pi(M)$ and $d\pi(S) \leftarrow d\pi(M)$ donation and acceptance characteristics, which differed significantly from those of Cl^-, PhO^-, and NHR^-.

In cases where RS^- groups include mercaptoamides the application of the above equation is more difficult because of the accidental degeneracy of the ν(NO) and the amide ν(CO) bands. This problem is encountered for the secondary amide complexes **3** and **5**, but not the tertiary amide complexes **4** and **6**, in which the nitrosyl band can be quite easily observed. (Figure 4, top) In the secondary amide complexes, however, the ν(NO) bands were detected by resonance Raman spectroscopy, using 488.0-nm excitation, which favors the enhancement of the ν(NO) fundamental band (Figure 4, bottom; Figure 5). In the series of complexes examined here the ν(NO) band shifts to higher frequency (Table 4) in concert with positive shifts in redox potential, probably due to a decrease of electron density in the metal coordination sphere. This would deprive the NO π^* orbitals of electron density, increase the N–O bond order, and thereby increase the force constant, as discussed by Obaidi et al.[40]

Cyclic Voltammetry. All of the complexes exhibit nearly reversible Mo(II)/Mo(III) redox couples in CH_3CN and MeOH solutions, and quasi-reversible couples in $CHCl_3$ (Table 5). The simple alkylthiolate complexes **1** and **2** serve as controls and reside close together at the low end of the redox potential scale with couples in CH_3CN solution at –0.940 and –0.960 V (relative to SCE), respectively. At the high end of the scale we find **3**, in CH_3CN, with a redox couple of –0.643 V (Figure 6). This positive shift of about 300 mV relative to the alkylthiolates is congruent with the results of several other studies that have suggested that N–H···S hydrogen bonding in Fe–S complexes is accompanied by positive redox potential shifts.[8-10,12] This is the first reported observation of a redox potential shift in a structurally characterized, hydrogen-bonding complex that incorporates an *alkylthiolate* ligand. The latter is free of the π orbital inductive effects that occur in hydrogen-bonded phenylthiolate ligands which have been employed in similar investigations.[14,35]

In **5**, the observation of a positive redox potential shift of +120 mV, in CH_3CN relative to **1**, was surprising since N–H···S hydrogen bonds are absent from **5** in either the solid or solution states. This result led us to investigate the redox influence of *N,N*-dimethylmercaptoamide ligands with their polar non-hydrogen-bonding groups. The latter induced large positive redox potential shifts relative to **1** and **2**, with redox couples of –0.740 and –0.750 V in **4** and **6**, respectively. *These positive shifts of ~200 mV clearly show that the polarity of the environment adjacent to a redox active site has a strong influence on the redox potential, similar in magnitude and direction to the effect of ligand hydrogen bonding.* This effect may be attributed

Table 4. Selected Vibrational Frequency (cm^{-1}) Data for $Mo[HB(Me_2pz)_3](NO)(SR)_2$[a]

SR group	ν(CO),[b] IR	ν(NO),[b] IR	ν(NO),[d] Raman
SBu (**2**)		1658[e]	1658
SEt (**1**)		1660	1661
$SC_2H_4CONHCH_3$ (**5**)	broad[c]	1662 (broad)[c]	1663
$SC_2H_4CON(CH_3)_2$ (**6**)	1643	1662	1664
$SCH_2CON(CH_3)_2$ (**4**)	1641	1669	1669
$SCH_2CONHCH_3$ (**3**)	broad[c]	1672 (broad)[c]	1671

[a] ν(CO) frequencies were determined for the neutral ligand in $CHCl_3$ solution by IR. They are $HSCH_2CONHCH_3$, 1666.1 cm^{-1}; $HSC_2H_4CONHCH_3$, 1669.5 cm^{-1}; $HSCH_2CON(CH_3)_2$, 1641.4 cm^{-1}; and $HSC_2H_4CON(CH_3)_2$, 1637.6 cm^{-1}. [b] Infrared data on complexes **3–6** were recorded in CH_2Cl_2 solution. [c] These frequencies represent a composite of overlapping ν(CO) and ν(NO) bands. [d] Data were recorded in CH_2Cl_2 solution, 488.0-nm excitation, 10-cm^{-1} spectral slit width. The frequencies are listed relative to the $\nu(CH_2)a_1$ 1425-cm^{-1} peak of CH_2Cl_2. In FTIR data, $\nu(CH_2)a_1$ has a frequency of 1422 cm^{-1}. [e] Ref 24; this work.

(39) Pickett, C. J. In *Comprehensive Coordination Chemistry*; Wilkinson, G., Ed.; Pergamon: New York, 1987; Vol. 1, pp 498–499.

(40) Obaidi, N. A.; Chaudhury, M.; Clague, D.; Jones, C. J.; Pearson, J. C., McCleverty, J. A.; Salam, S. S. *J. Chem. Soc., Dalton Trans.* **1987**, 1733–1736.

Table 5. Cyclic Voltammetry Results for Selected Complexes $Mo[HB(Me_2pz)_3](NO)(SR)_2$, $E_{1/2}$ (V),[a] ΔE (mV)[b]

	CH_3CN		MeOH		$CHCl_3$	
SR group	$E_{1/2}$	ΔE	$E_{1/2}$	ΔE	$E_{1/2}$	ΔE
SBu (2)	−0.960	75	−0.813	75	−1.008	135
SEt (1)	−0.940	100	−0.800	120	−0.968	135
$SC_2H_4CONHCH_3$ (5)	−0.820	110	−0.688	75	−0.728	195
$SC_2H_4CON(CH_3)_2$ (6)	−0.750	70	−0.633	75	−0.710	125
$SCH_2CON(CH_3)_2$ (4)	−0.740	110	−0.605	60	−0.713	105
$SCH_2CONHCH_3$ (3)	−0.643	85	−0.558	65	−0.563	155

[a] All data are reported relative to SCE (CH_3CN, MeOH) or Ag ($CHCl_3$). Scan rate: 50 mV/s. electrolyte: 0.10 M Et_4NClO_4 in CH_3CN, 0.20 M Bu_4NBF_4 in MeOH, and 0.30 M Bu_4NPF_6 in $CHCl_3$. Electrodes: (i) in CH_3CN and MeOH, working electrode glassy carbon, counter electrode Pt wire, reference electrode saturated calomel; (ii) in $CHCl_3$, working electrode Pt wire, counter electrode Pt wire, reference electrode Ag wire. $E_{1/2}$ ferrocene (solvent/ref electrode): +0.380 (CH_3CN/SCE); +0.433 (MeOH/SCE); +0.530 ($CHCl_3$/Ag); +0.555 (CH_3CN/Ag). [b] ΔE is the peak-to-peak separation of the cathodic and anodic peaks. $\Delta E_{ferrocene}$ = 80–85 mV in CH_3CN or MeOH and 160 mV in $CHCl_3$.

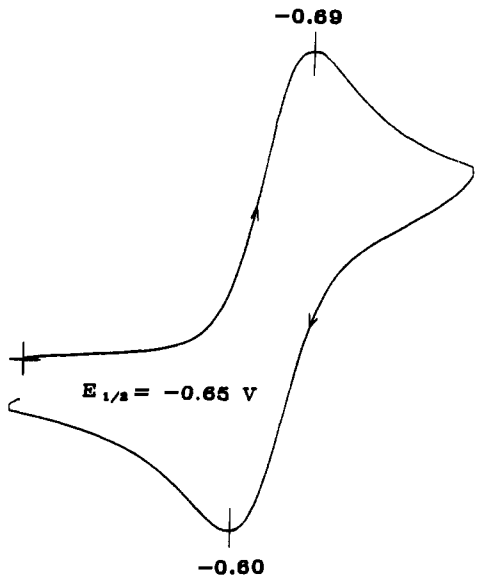

Figure 6. Cyclic voltammogram of $Mo[BH(Me_2pz)_3](NO)(SCH_2CONHCH_3)_2$ (3) (1.0 mM) in acetonitrile. Data were collected at room temperature using a glassy carbon working electrode, Pt wire counter electrode, and saturated calomel reference electrode, with a scan rate of 50 mV/s and Et_4NClO_4 (0.10 M) as electrolyte.

charge–dipole interactions between the amide group and the atoms of the Mo coordination shell.

The solvents in which voltammetric data were acquired have different acceptor numbers (AN): $CHCl_3$ (23.1), CH_3N (19.3), and CH_3OH (41.3) (Table 5). The acceptor number provides a measure of the Lewis acidity. The redox potentials of complex ions have been shown to increase in proportion to solvent AN.[41] This occurs because the reduced complex is stabilized by forming a Lewis acid–base pair with the solvent. As the solvent AN increases, so too does the stability of the pair relative to an acid–base pair formed by the oxidized complex and the solvent. The effect of AN on redox potential has been reported for several tetranuclear cubane-like clusters (Fe_4S_4), with the predominant interaction evidently occurring between the solvent and the sulfur ligands.[42] The redox potentials in Table 5 show a complex relationship with AN for the three solvents. Acceptor number is clearly not the only factor that determines the redox potentials in the complexes **1–6**. Among other things one might include steric effects or ligand-binding geometry as important factors that could determine the strength of the solvent–ligand interaction.

Iron–sulfur centers of the type $Fe(SR)_4^{1-/2-}$, $Fe_2S_2(SR)_4^{2-/3-}$, and $Fe_4S_4(SR)_4^{1-/2-/3-}$, where R = H and CH_3, have been investigated by quantum mechanical and density functional methods.[43,44] Because of the extent of covalency in the Fe–S bonds, more than half of the charge of an electron added to the complex is taken up by the sulfur, with most of the remainder on the Fe atoms. Similarly, in the Mo(II) reduced state of complexes **1–6**, the added electron, rather than remaining localized on Mo, is probably delocalized among the atoms of the Mo–N_{pz},NO,S coordination sphere. In the amide-containing complexes, **3–6**, this electron distribution in the reduced state probably results in enhanced *intraligand* charge–dipole interactions between coordinated sulfur, with their increased partial negative charge, and the tethered amide groups. Such interactions would explain the positive redox potential shifts observed in complexes **3–6**, relative to the redox potentials of **1** and **2**. Dipole–dipole interactions have been shown to promote pairing of polar molecules in solution. For example *N*,*N*-dimethylformamide and acetonitrile have been reported to form dipole–dipole pairs with their dipoles arranged in an antiparallel orientation.[45,46] Charge–dipole interactions are stronger than dipole–dipole interactions[47] and might plausibly be expected to account for the redox potential shifts in the mercaptoamide complexes.

Recent theoretical investigations by Stephens and co-workers[48] provide support for the idea that, in the Fe_4S_4 proteins Fd (ferredoxin) and HiPIP (high-potential iron–sulfur protein), the polarity of the redox active-site environment is important in the regulation of redox potentials. Our results support this view and show that the polarity of the environment around a redox active site is perhaps as *important* as the formation of ligand hydrogen bonds in the regulation of redox potentials. These results highlight the electrostatic nature of the hydrogen bonding[49] and suggest that the principal effect of *N*-H···S hydrogen bonds is to bring polar amide groups into close proximity to the redox active site. In principle, this effects the formation of charge–dipole pairs that are more closely associated than would be possible for a non-hydrogen-bonding polar group. This arrangement would explain the occurrence of significant positive redox potential shifts relative to a control complex in an environment of low polarity.

In discussing the influence of amide substituents on sulfur in **3–6**, we must take into account the two possible pathways of interaction, which may be either through-space or through-bond. Interaction by the first pathway has been designated as a *field effect*, which involves an electrostatic interaction. The second pathway, which involves the polarization of σ bonds, gives rise

(41) Gutmann, V. *The Donor-Acceptor Approach to Molecular Interactions*; Plenum: New York, 1978; pp 29, 127–129.
(42) Kodaka, M.; Tomohiro, T. *Chem. Express* **1990**, *5*, 97–100.
(43) Noodleman, L.; Case, D. A. In *Advances in Inorganic Chemistry*; Cammack, R., Sykes, A. G., Eds.; Academic Press: New York, 1992; Vol. 38, pp 424–470.
(44) Noodleman, L.; Norman, J. G., Jr.; Osborne, J. H.; Aizman, A.; Case, D. *J. Am. Chem. Soc.* **1985**, *107*, 3418–3426.
(45) Radnai, T.; Itoh, S.; Ohtaki, H. *Bull. Chem. Soc. Jpn.* **1988**, *61*, 3845–3852.
(46) Sharma, A. K.; Sharma, D. R.; Gill, D. S. *J. Phys. D: Appl. Phys.* **1985**, *18*, 1199–1206.
(47) Israelachvili, J. N. *Intermolecular and Surface Forces*; Academic Press: San Diego, 1991; Chapter 4.
(48) Langen, R.; Jensen, G. M.; Jacob, U.; Stephens, P. J.; Warshel, A. *J. Biol. Chem.* **1992**, *267*, 25625–25627.
(49) Pimentel, G. C.; McClellan, A. L. *The Hydrogen Bond*; Freeman: San Francisco, 1960; pp 229–237.

to the well-known *inductive effect*. Recent experimental and theoretical studies of numerous saturated aliphatic compounds[21,50] support a field effect mechanism for distal interactions, very nearly to the complete exclusion of an inductive mechanism. In particular, Reynolds[21,51] has shown that the field effect fully explains the influence of a substituent X on the acidity of substituted acetic acid XCH_2CO_2H. The inductive effect, which is negligible in acetic acid, can be ignored in longer alkyl chain carboxylic acids with substitution at the terminal position. In the series of compounds discussed in our work, **1–6**, the likelihood is that the interaction between coordinated sulfur and amide ligand terminal groups would be exclusively electrostatic (through-space) in nature.

Conclusion

The observed effect of N–H···S hydrogen bonds on the redox potential of complex **3** may indeed be sufficient to explain the differences in the stable redox couples of $Fd^{2-/3-}$, which has eight N–H···S hydrogen bonds, and $HiPIP^{1-/2-}$, which has five, where the redox potentials are in the range –645 to –280 mV for Fd and 50 to 450 mV for HiPIP.[2] Further, it may serve to explain the redox potential difference of approximately 950 mV between Rd (rubredoxin) in water (–0.05 V) and the simple iron tetrathiolate complexes in organic solvents (–1.0 V).[52-56] However, differences in N–H···S hydrogen bonding does not explain the variations in redox potentials within separate families of proteins, Fd, HiPIP, and Rd. The cause of these variations might be explained by the observation of redox and ν(NO) frequency shifts in complexes **4**, **5**, and **6** (relative to **1** and **2**). The redox potential and accompanying frequency shifts in these synthetic complexes suggest that the electronic structure at the active site is quite susceptible to nonbonding electrostatic effects. Similar effects adjacent to the active sites in electron transfer Fe–S proteins might explain the range of redox potentials observed among members of a single family, e.g., ~365 mV in Fd and ~400 mV in HiPIP.[2]

In summary, in the $Mo[HB(Me_2pz)_3](NO)(SR)_2$ complexes discussed here (i) N–H···S hydrogen bonding causes a positive shift in redox potential on the order of several hundered millivolts in complexes where amide-thiolate π conjugation is absent, and (ii) redox potential shifts of the same order of magnitude are apparently induced by charge–dipole interactions. These results show two types of interactions that may account for differences in redox potential and stability observed in Fe–S proteins with structurally similar active sites.

Acknowledgment. We thank Professors J. Dannenberg and P. Lindahl, Dr. E. Stiefel, and Professor A. Warshel for helpful discussions. This investigation has been supported by grants from the EXXON Education Foundation and the National Science Foundation (Grant No. CHE-9203455) to M.A.W.

Supplementary Material Available: Tables of complete data collection information, atomic coordinates, bond distances, bond angles, anisotropic thermal parameters, and positional parameters of the H atoms for both **3** and **5** as well as a stereo packing diagram of **5** (18 pages); structure factor tales for **3** and **5** (29 pages). This material is contained in many libraries on microfiche, immediately follows this article in the microfilm version of the journal, and can be ordered from the ACS; see any current masthead page for ordering information.

(50) Bowden, K. *J. Chim. Phys.* **1992**, *89*, 1647–1659.
(51) Reynolds, W. F. *J. Chem. Soc., Perkin Trans. 2* **1980**, 985–992.
(52) Lovenberg, W.; Sobel, B. E. *Proc. Natl. Acad. Sci. U.S.A.* **1965**, *54*, 193–199.
(53) Peterson, J. A.; Coon, M. J. *J. Biol. Chem.* **1968**, *243*, 329–334.
(54) Lane, R. W. Ibers, J. A.; Frankel, R. B.; Holm, R. H. *Proc. Natl. Acad. Sci. U.S.A.* **1975**, *72*, 2866–2872.
(55) Lane, R. W. Ibers, J. A.; Frankel, R. B.; Papaefthymiou, G. C.; Holm, R. H. *J. Am. Chem. Soc.* **1977**, *99*, 84–98.
(56) Moura, I.; Moura, J. J. G.; Santos, M. H.; Xavier, A. V.; LeGall, J. *FEBS Lett.* **1979**, *107*, 419–421.